Letter

Dynamics of crack front waves in three-dimensional material failure

Sanhita Das [*], Yuri Lubomirsky,[*] and Eran Bouchbinder [†]

Chemical and Biological Physics Department, Weizmann Institute of Science, Rehovot 7610001, Israel

Crack front waves (FWs) are dynamic objects that propagate along moving crack fronts in three-dimensional (3D) materials. We study FW dynamics in the framework of a 3D phase-field platform that features a rate-dependent fracture energy $\Gamma(v)$ (v is the crack propagation velocity) and intrinsic length scales, and quantitatively reproduces the high-speed oscillatory instability in the quasi-2D limit. We show that in-plane FWs feature a rather weak time dependence, with decay rate that increases with $d\Gamma(v)/dv > 0$, and largely retain their properties upon FW-FW interactions, similarly to a related experimentally observed solitonic behavior. Driving in-plane FWs into the nonlinear regime, we find that they propagate slower than predicted by a linear perturbation theory. Finally, by introducing small out-of-plane symmetry-breaking perturbations, coupled in- and out-of-plane FWs are excited, but the out-of-plane component decays under pure tensile loading. Yet, including a small antiplane loading component gives rise to persistent coupled in- and out-of-plane FWs.

Introduction. Material failure is a highly complex phenomenon, involving multiple scales, strong spatial localization and nonlinear dissipation. It is mediated by the propagation of cracks, which feature nearly singular stresses near their edges [1,2]. In brittle materials, they reach velocities comparable to elastic wave speeds, hence also experience strong inertial effects. In thin, quasi-two-dimensional (2D) samples, a crack is viewed as a nearly singular point that propagates in a 2D plane and leaves behind it a broken line. In thick, fully-3D samples, a crack is a nearly singular front (line) that evolves in a 3D space and leaves behind it a broken surface. While significant recent progress has been made in understanding dynamic fracture in 2D [3–6], our general understanding of dynamic fracture in 3D remains incomplete [7–36].

A qualitative feature that distinguishes 2D from 3D material failure is the emergence of crack front waves (FWs) in the latter. FWs are compact objects that persistently propagate along crack fronts [8–15]. In the most general case, FWs feature both a component in the main crack plane and an out-of-plane component [12–14]. A linear perturbation theory of singular tensile cracks, featuring no intrinsic length scales and rate-independent fracture-related dissipation, predicts the existence of non-dispersive in-plane FWs, whose velocity is close to the Rayleigh wave speed $c_{\rm R}$ [9,10]. An extended linear perturbation theory also predicts the existence of non-dispersive out-of-plane FWs in the same velocity range [25], albeit to linear order the in- and out-of-plane components are decoupled.

Here, we study FWs in a 3D theoretical-computational framework that has recently quantitatively predicted the high-speed oscillatory instability in 2D [4–6]. It is based on a phase-field approach to fracture [37–44], where large
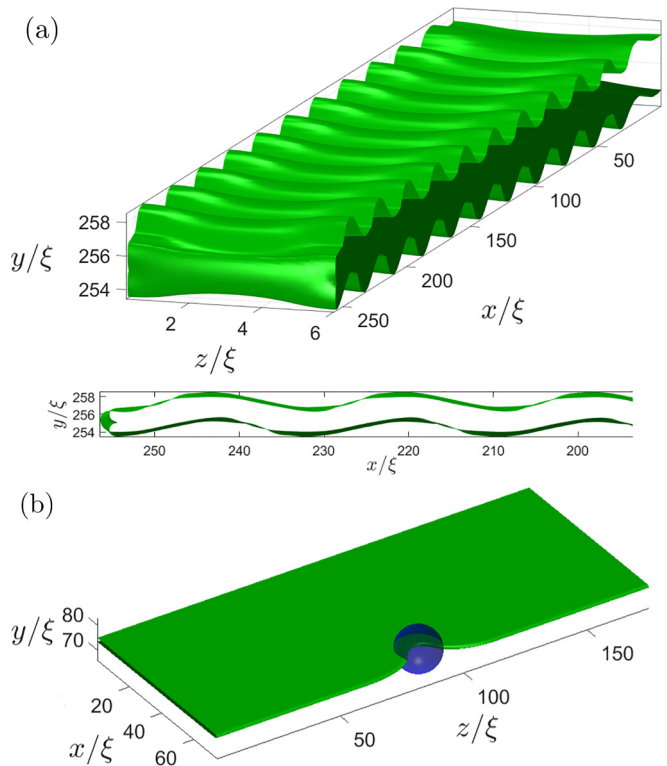
FIG. 1. (a) The high-speed oscillatory instability observed in 3D phase-field simulation with $L_z = 6\xi$. The crack propagates in the x direction, a tensile (mode I) loading is applied in the y direction and traction-free boundary conditions are employed in z. Plotted is the phase-field $\phi(\boldsymbol{x}, t) = 1/2$ isosurface, which is associated with a finite crack width, as demonstrated in the lower inset, where a side view of the crack is presented. (b) A steady-state planar crack under tensile loading in a thick 3D system (with periodic boundary conditions in z) interacts with a tough spherical asperity, whose center here coincides with the crack plane, $y = L_y/2$ (see text for additional details).

---

[*]These authors contributed equally to this work.

[†]eran.bouchbinder@weizmann.ac.il
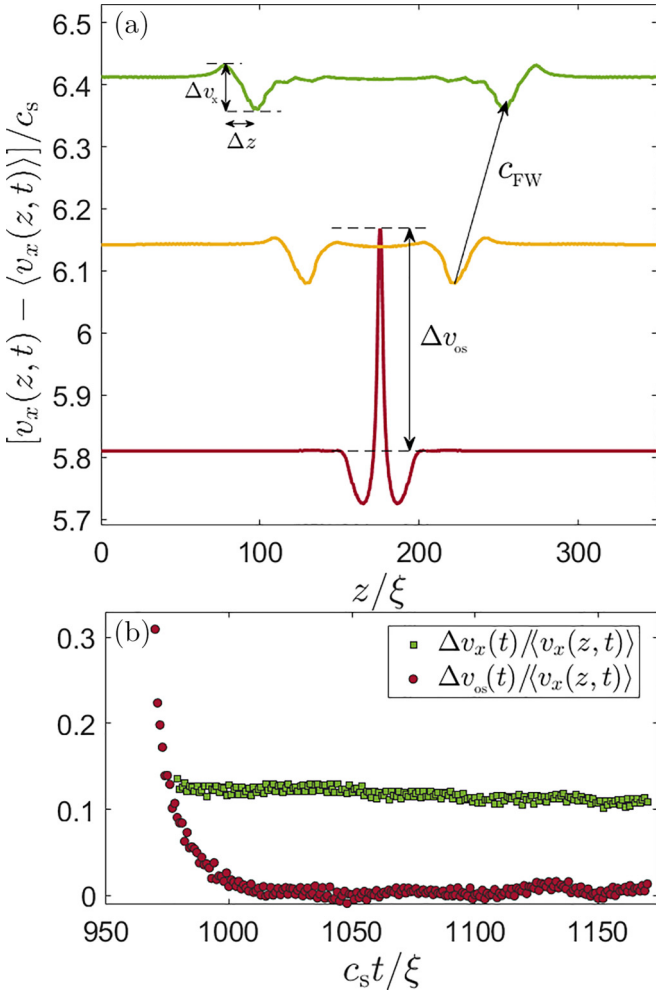
FIG. 2. (a) Equal time interval snapshots of $v_x(z,t) - \langle v_x(z,t)\rangle$ (normalized and shifted for visual clarity [45]) during in-plane FWs formation and propagation (time snapshots correspond to $t=968, 1023, 1068\, \xi/c_s$). The velocity overshoot Δv_{os}, and FW amplitude Δv_x, width Δz and propagation velocity c_{FW} are all marked (see also text). FWs were generated using $v=0.6c_s$, $R=6\xi$, and $\delta\Gamma=0.6$, and feature $c_{FW}=0.977c_R$. (b) $\Delta v_{os}(t)/\langle v_x(z,t)\rangle$ and $\Delta v_x(t)/\langle v_x(z,t)\rangle$ (see legend).

scale elastic deformations—described by an elastic energy density $e(\boldsymbol{u})$ (here $\mathbf{u}(\boldsymbol{x},t)$ is the displacement field)—are coupled on smaller scales near the crack edge to an auxiliary scalar field—the phase-field $\phi(\mathbf{x},t)$—that mathematically mimics material breakage. The main merit of the approach is that the dissipative dynamics of $\phi(\boldsymbol{x},t)$ spontaneously generate the traction-free boundary conditions defining a crack, and consequently select its trajectory and velocity v. Moreover, it also incorporates intrinsic length scales near the crack edge—most notably a dissipation length ξ (sometimes termed the "process zone" size [1,2]) and possibly a nonlinear elastic length ℓ_{nl} (embodied in $e(\boldsymbol{u})$ [3–6])—absent in singular crack models, and a rate-dependent fracture energy $\Gamma(v)$ that accompanies the regularization of the edge singularity.

The theoretical-computational framework and the quasi-2D limit. We consider a homogeneous elastic material in 3D, where L_z is the thickness in the z direction, L_y is the height

in the tensile loading y direction and x is the crack propagation direction (we employ a treadmill procedure to obtain very long propagation distances using a finite simulation box length L_x [6]). We use a constitutively linear energy density $e(\boldsymbol{u}) = \frac{1}{2}\lambda\, \mathrm{tr}^2(\boldsymbol{E}) + \mu\, \mathrm{tr}(\boldsymbol{E})$, with Lamé coefficients λ and μ (shear modulus), and where $\boldsymbol{E} = \frac{1}{2}[\nabla\boldsymbol{u}+(\nabla\boldsymbol{u})^{\mathrm{T}}+(\nabla\boldsymbol{u})^{\mathrm{T}}\nabla\boldsymbol{u}]$ is the Green-Lagrange metric strain tensor. The latter ensures rotational invariance, yet it introduces geometric nonlinearities (last term on the right-hand side). However, the associated nonlinear elastic length scale ℓ_{nl} remains small (unless otherwise stated [45]), such that we essentially consider a linear elastic material and the dissipation length ξ is the only relevant intrinsic length scale. The latter emerges once $e(\boldsymbol{u})$ is coupled to the phase-field $\phi(\boldsymbol{x},t)$ [4–6].

Applying this framework in 2D, i.e., $L_z=0$, the high-speed oscillatory instability was predicted, in quantitative agreement with thin-sample experiments [3–6,54–56]. In this instability, a straight crack loses stability in favor of an oscillatory crack when surpassing a critical velocity close to c_R (to be distinguished from the qualitatively different quasistatic oscillatory instability [46–53]). In Fig. 1(a), we present a high-speed oscillatory instability in a thin 3D material, $L_z>0$, where all quantities—including the wavelength of oscillations—agree with their 2D counterparts. These results support the validity of the 3D framework as it features the correct quasi-2D limit.

Next, we aim at exciting FWs and studying their dynamics. We consider thick systems (with $L_z/\xi \gg 1$ and periodic boundary conditions along z), see Fig. 1(b). Loading boundary conditions $u_i(x, y=0, z)$ and $u_i(x, y=L_y, z)$ are applied. In most, but not all, cases (see below), we apply tensile boundary conditions $u_y(x, y=0, z) = -u_y(x, y=L_y, z) = \delta/2$, resulting in mode I cracks initially located at the $y= L_y/2$ plane. The tensile strain δ/L_y translates into a crack driving force G (energy release rate) [1,2,17], which is balanced by a rate-dependent fracture energy $\Gamma(v)$. The latter features $d\Gamma(v)/dv>0$, whose magnitude depends on the relaxation/dissipation time scale τ of the phase-field ϕ [6], through the dimensionless parameter $\beta \equiv \tau c_s/\xi$ (where c_s is the shear wave speed). The entire theoretical-computational framework depends on two dimensionless parameters, β and e_c/μ, where e_c is the onset of dissipation energy density [6].

FWs are excited by allowing a steady-state crack front to interact with tough spherical asperities (one or more), see Fig. 1(b). Each spherical asperity is characterized by a radius R and a dimensionless fracture energy contrast $\delta\Gamma \equiv \Delta\Gamma/\Gamma_0 > 0$, where $\Gamma_0 \equiv \Gamma(v\to 0)$. The position of the asperities with respect to the crack plane, $y=L_y/2$, determines the type of perturbation induced, i.e., in-plane or coupled in- and out-of-plane perturbations. The resulting perturbed crack front is then described by an evolving line $\boldsymbol{f}(z,t)=(f_x(z,t), f_y(z,t))$ parameterized by the z coordinate and time t (assuming no topological changes take place). Here, $f_x(z,t)$ is the in-plane component and $f_y(z,t)$ is the out-of-plane component, and an unperturbed tensile crack corresponds to $\boldsymbol{f}(z,t)=(vt, 0)$.

The dynamics of in-plane FWs. In-plane FWs are excited by placing a single asperity whose center coincides with the crack plane, $y=L_y/2$ [cf. Fig. 1(b)]. The tough asperity locally retards the crack front, leading to a local increase in the front curvature and G [7,27]. The front then breaks the asperity [cf. Fig. 1(b)], leading to a subsequent velocity overshoot $\Delta v_{os}(t)$
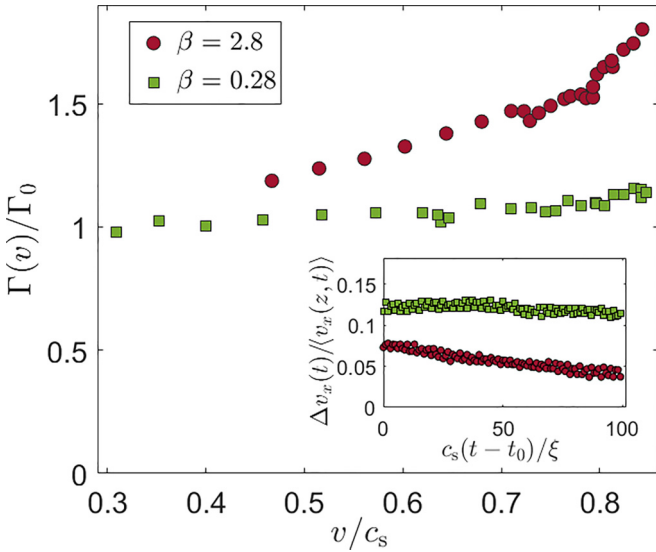
FIG. 3. $\Gamma(v)/\Gamma_0$ for $\beta=0.28$ (green squares) and $\beta=2.8$ (brown circles) as previously obtained in 2D (data as in Fig. 3a in [6]), where $d\Gamma(v)/dv$ differs by a factor of 4.6. (inset) The corresponding dimensionless FW amplitude $\Delta v_x(t)/\langle v_x(z,t)\rangle$ for both $\beta=0.28$ (green squares) and $\beta=2.8$ (brown circles) for $v=0.6c_s$ (FWs were generated using $R=6\xi$ and $\delta\Gamma=0.6$). In both cases, $\Delta v_x(t)/\langle v_x(z,t)\rangle \sim 1-(t-t_0)/T$, where $1/T$ differs by a factor of 5.8 (see text for details and discussion). t_0 is the time at which well-defined FWs first exist.

ahead of the asperity (cf. Fig. 2(a)). To quantify in-plane FWs dynamics, we employ $v_x(z,t) \equiv \partial_t f_x(z,t)$, typically with respect to $\langle v_x(z,t)\rangle \approx v$, where $\langle \cdot \rangle$ corresponds to an average along z (unless otherwise stated). Strictly speaking, the physically relevant quantity is the normal front velocity, $v_\perp(z,t)= v_x(z,t)/\sqrt{1+(\partial_z f_x(z,t))^2}$. However, for our purposes here $v_x(z,t)$ itself is sufficient.

After $\Delta v_{os}(t)$ reaches a maximum, it decays to zero (cf. Fig. 2(b)) and a pair of in-plane FWs is generated. Each FW features an amplitude $\Delta v_x(t)$ (defined as the crest-to-trough difference), a width $\Delta z(t)$ (the corresponding crest-to-trough z distance) and a propagation velocity c_{FW} (in the laboratory frame of reference), all marked in Fig. 2(a). The dimensionless FW amplitude $\Delta v_x(t)/\langle v_x(z,t)\rangle$ is plotted in Fig. 2(b). The FW inherits its scale from R, as shown in Ref. [45].

A linear perturbation theory [9], developed to leading order in $|\partial_z f_x(z,t)| \ll 1$, predicted the existence of nondispersive in-plane FWs, in the absence of intrinsic length scales ($\xi \rightarrow 0$) and for a rate-independent fracture energy ($d\Gamma(v)/dv = 0$). The theory predicts $0.94 < c_{FW}(v)/c_R < 1$ (when v varies between 0 and c_R). These predictions have been subsequently supported by boundary-integral method simulations of a rate-independent cohesive crack model [10]. In Ref. [9], an effective crack propagation equation of motion has been conjectured for the $d\Gamma(v)/dv \neq 0$ case, suggesting that for $d\Gamma(v)/dv > 0$ in-plane FWs undergo some form of attenuation during propagation.

As materials feature a rate-dependent fracture energy $\Gamma(v)$, it is important to shed light on this physical issue. Our framework naturally enables it as $d\Gamma(v)/dv$ is directly controlled by β. The evolution of the FW amplitude $\Delta v_x(t)/\langle v_x(z,t)\rangle$
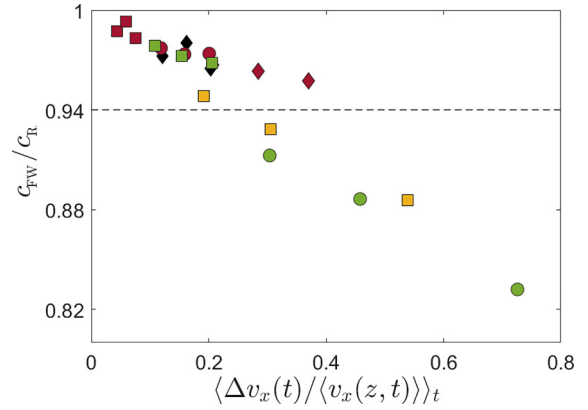
FIG. 4. c_{FW}/c_R vs $\langle \Delta v_x(t)/\langle v_x(z,t)\rangle\rangle_t$ ($\langle \cdot \rangle_t$ is a time average, prior to FW-FW interaction effects). The FW generation parameters: $v=0.5c_s$ (diamonds), $v=0.6c_s$ (circles), $v=0.7c_s$ squares, $R=4\xi$ (black), $R=6\xi$ (brown), $R=12\xi$ (green), $R=18\xi$ (orange). For fixed v and R, $\langle \Delta v_x(t)/\langle v_x(z,t)\rangle\rangle_t$ increases with $\delta\Gamma$ [45].

presented in Fig. 2 corresponds to very weak rate dependence, shown in Fig. 3(a) for $\beta=0.28$. Such a flat $\Gamma(v)$ is characteristic of nearly ideally brittle materials such as silica glass (cf. the experimental data in Fig. 2b of Ref. [57]). $\Delta v_x(t)/\langle v_x(z,t)\rangle$ in this case, presented again in the inset of Fig. 3, reveals a weak linear attenuation proportional to $1-(t-t_0)/T$, where $c_s T/\xi \simeq 1210$. However, while our system width L_z is large enough to resolve FW propagation distances several times larger than their characteristic width Δz (cf. Fig. 2(a)), the overall propagation time Δt prior to FW-FW interaction (through the periodic boundary condition, to be discussed below) is $\Delta t \sim \mathcal{O}(100)$ (cf. Fig. 2(b)), implying $\Delta t \ll T$. Consequently, the presented results cannot tell apart an exponential decay from a linear one as $\exp[-\Delta t/T] \simeq 1 - \Delta t/T$ for $\Delta t \ll T$.

To address this point, and more generally the effect of the magnitude of $d\Gamma(v)/dv$ on in-plane FW dynamics, we increased β by an order of magnitude, setting it to $\beta=2.8$. The resulting $\Gamma(v)$, shown in Fig. 3 (previously reported for our model in 2D [6]), indeed reveals a significantly larger $d\Gamma(v)/dv$, nearly a factor 5 larger than that for $\beta=0.28$. The emerging $d\Gamma(v)/dv$ is similar to the one observed in brittle polymers (e.g., PMMA, cf. Fig. 2a in Ref. [57]) and in brittle elastomers (e.g., polyacrylamide, cf. Fig. 2B in Ref. [58]). The corresponding $\Delta v_x(t)/\langle v_x(z,t)\rangle$ is shown in the inset of Fig. 3, again following a linear attenuation proportional to $1-(t-t_0)/T$, this time with $c_s T/\xi \simeq 208$. Since in this case Δt is comparable to T, the results support a linear decay, in turn implying that in-plane FWs may propagate many times their characteristic width Δz even in materials with a finite $d\Gamma(v)/dv$. Moreover, we note that the decay rate $1/T$ varies between the two β values by a factor that is comparable to the corresponding variability in $d\Gamma(v)/dv$, indeed suggesting a relation between these two physical quantities [9].

We next consider the FW velocity c_{FW} and the possible effect of $\Delta v_x(t)/\langle v_x(z,t)\rangle$ on it. As explained above, the linear perturbation theory of Ref. [9] predicts $0.94 < c_{FW}/c_R < 1$. Consequently, we expect our excited in-plane FWs to feature c_{FW}/c_R within this range when $\Delta v_x(t)/\langle v_x(z,t)\rangle$ is small.
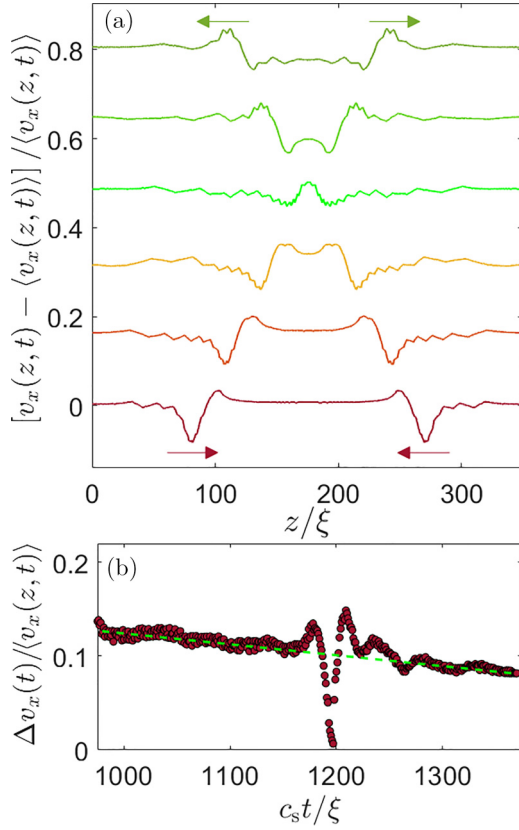
FIG. 5. (a) Equal time interval snapshots (see y axis label) revealing the interaction of the two FWs previously shown in Fig. 2(a). For improved visibility, we rotate the system along the z axis by $L_z/2$ such that the interaction event takes place in the middle of the system. (b) $\Delta v_x(t)/\langle v_x(z,t)\rangle$ for the dynamics shown in panel (a), the dashed line is a guide to the eye. See text for discussion.

FIG. 6. A pair of coupled in- and out-of-plane FWs triggered for $v=0.4c_s$ and $\beta=0.28$ using two adjacent asperities, each characterized by $R=6\xi$ and $\delta\Gamma=0.4$. To generate an out-of-plane perturbation, one asperity is shifted by $(\delta y=-2\xi, \delta z=-2\xi)$ relative to the middle of the crack front and the other by $(\delta y=2\xi, \delta z=2\xi)$. A small antiplane loading component is included, resulting in a mode-mixity (mode III/I) level of 3% (see text for discussion). Plotted are $f_y(z,t)$ (solid green lines, multiplied by 10, see left y axis) and $f_x(z,t)$ (dashed brown lines, right y axis) at equal time intervals. FWs persist through a FW-FW interaction, here taking place at the edges ($z=0, 350\xi$) and propagate at $c_{FW}=0.961c_R$.

This is indeed the case in Fig. 4, where the dimensionless FW amplitude is controlled by systematically varying v, and the asperity parameters R and $\delta\Gamma$ (in fact, we find that the amplitude varies linearly with $\delta\Gamma$ for fixed v and R [45]). However, when the amplitude is no longer small, apparently beyond the linear perturbation regime, we find that c_{FW}/c_R decreases below 0.94, indicating that nonlinear effects tend to slow down in-plane FWs.

Finally, we take advantage of the z-periodic boundary conditions to study FW-FW interactions. In Fig. 5(a), we present the interaction dynamics between the in-plane FWs previously shown in Fig. 2(a). It is observed that the FWs retain their overall shape after the interaction, yet during the interaction they do not feature a linear superposition. This behavior is quantified in Fig. 5(b), where $\Delta v_x(t)/\langle v_x(z,t)\rangle$ is plotted before, during and after FW-FW interaction (before and after the interaction it is identical for the two noninteracting FWs). In this case, it is observed that before and after the FW-FW interaction, each FW follows the very same weak linear decay previously presented in Fig. 2(b) (see superimposed dashed line) and nearly drops to zero during the interaction. This solitonlike behavior is reminiscent of similar experimental observations made in relation to coupled in- and out-of-plane FWs [12–14], which are discussed next.

Coupled in- and out-of-plane FWs. Experimentally, FWs have been observed through their fractographic signature on postmortem fracture surfaces [12–15], i.e., the observed FWs featured nonlinearly coupled in- and out-of-plane components, where both $f_x(z,t)$ and $f_y(z,t)$ are nonzero and apparently propagate at the same c_{FW}. FWs in the experiments were excited by huge perturbations, 3–4 orders of magnitude larger than the out-of-plane component of the generated FWs [13,14], which in itself was comparable to the fracture dissipation length ξ. For example, asperity sizes of $100-1000\,\mu m$ gave rise to FWs with an out-of-plane component of $0.1\,\mu m$ in silica glass [13], whose fracture dissipation (process zone) size is estimated to be in the tens of nanometers range [59]. Coupled in- and out-of-plane FWs are also spontaneously triggered by microbranching events [14,15], likely to be "large perturbations" as well.

Due to computational limitations—most notably on the magnitude of L_y—we are not able to resolve this huge span in scales between the triggering perturbation and the resulting out-of-plane component. Consequently, the out-of-plane perturbations accessible to us are rather small. In particular, we perturbed the initially planar crack by a pair of adjacent asperities, one slightly shifted above the crack plane and one below, breaking the up-down symmetry. Such perturbations excite both in- and out-of-plane crack front components, but

the latter decays after a short transient (while the former persists [45]).

To understand if the latter observation is exclusively due to computational limitations (in resolving finite perturbations and the associated scale separation) or whether other physical factors are at play, we considered the recent experiments of Ref. [35]. It was shown therein that out-of-plane crack surface structures—most notably surface steps [31,35,36]—might crucially depend on the existence of small, weakly experimentally controlled, antiplane loading component (mode III, anti-symmetric loading in the z direction, e.g., due to small misalignment between the crack plane and the tensile axis). To test the possibility that a small amount of mode-mixity (mode III/I) might play a role in generating persistent coupled in- and out-of-plane FWs, we introduced a mode-mixity level of 3%, i.e., $u_z(x, y=0, z) = -u_z(x, y=L_y, z) = 0.03 |u_y(x, y=L_y, z)|$ into the above-described calculations. The results are presented in Fig. 6, revealing persistent propagation of a pair of coupled in- and out-of-plane FWs, featuring nonzero $f_x(z,t)$ and $f_y(z,t)$ that propagate at $c_{FW} = 0.961c_R$.

The amplitude of $f_y(z,t)$ is tiny, a small fraction of ξ (yet it varies systematically with mode-mixity [45]). Moreover, it is an order of magnitude small than that of $f_x(z,t)$ (notice the two y axis labels in Fig. 6). Interestingly, this observation is consistent with experimental estimates [13] that suggest that $\partial_t f_y(z,t)$ is much smaller than $\partial_t f_x(z,t)$ (estimated using real-time measurements of in-plane crack velocity fluctuations at $z=0$ and $z=L_z$ [13]). Overall, the observed coupled in- and out-of-plane FWs propagating at $c_{FW} = 0.961c_R$ with a small out-of-plane component, which also persist through FW-FW interactions, is reminiscent of several key experimental findings [12–14]. It remains to be seen whether a small mode-mixity, which is physically realistic, is an essential ingredient. One manifestation of it, which can be tested experimentally, is that the out-of-plane amplitude of the pair of FWs has opposite signs, see Fig. 6.

Summary and outlook. Our results demonstrate that the same framework that quantitatively predicts the high-speed oscillatory instability in thin materials, also provides deep insight into FW dynamics in thick, fully 3D materials. The effect of realistic rate-dependent fracture energy $d\Gamma(v)/dv > 0$ on the propagation of in-plane FWs is elucidated, as well as their solitonic nature and the effect of nonlinear amplitudes on their velocity. Persistent coupled in- and out-of-plane FWs, similar to experimental observations, are demonstrated once a small antiplane (mode III) loading component is added to the dominant tensile (mode I) loading component.

Our findings give rise to pressing questions and subsequent investigation directions, most notably in relation to out-of-plane crack structures such as microbranching events and surface faceting [17,31]. The roles of mode-mixity fluctuations in nominally tensile failure and of realistic material disorder/heterogeneity (we focused on homogeneous materials, discrete asperities were just introduced to generate FWs) should be particularly considered. In addition, improved computational capabilities (e.g., based on multi-GPU implementations) should be developed in order to obtain better scale separation, which in turn may allow one to understand the effect of finite out-of-plane perturbations on 3D crack dynamics.

[1] L. B. Freund, *Dynamic Fracture Mechanics* (Cambridge University Press, Cambridge, 1990).

[2] K. R. Broberg, *Cracks and Fracture* (Academic Press, New York, 1999).

[3] E. Bouchbinder, T. Goldman, and J. Fineberg, The dynamics of rapid fracture: Instabilities, nonlinearities and length scales, Rep. Prog. Phys. **77**, 046501 (2014).

[4] C.-H. Chen, E. Bouchbinder, and A. Karma, Instability in dynamic fracture and the failure of the classical theory of cracks, Nat. Phys. **13**, 1186 (2017).

[5] Y. Lubomirsky, C.-H. Chen, A. Karma, and E. Bouchbinder, Universality and stability phase diagram of two-dimensional brittle fracture, Phys. Rev. Lett. **121**, 134301 (2018).

[6] A. Vasudevan, Y. Lubomirsky, C.-H. Chen, E. Bouchbinder, and A. Karma, Oscillatory and tip-splitting instabilities in 2D dynamic fracture: The roles of intrinsic material length and time scales, J. Mech. Phys. Solids **151**, 104372 (2021).

[7] J. Rice, First-order variation in elastic fields due to variation in location of a planar crack front, J. Appl. Mech. **52**, 571 (1985).

[8] J. Willis and A. Movchan, Three-dimensional dynamic perturbation of a propagating crack, J. Mech. Phys. Solids **45**, 591 (1997).

[9] S. Ramanathan and D. S. Fisher, Dynamics and Instabilities of Planar Tensile Cracks in Heterogeneous Media, Phys. Rev. Lett. **79**, 877 (1997).

[10] J. W. Morrissey and J. R. Rice, Crack front waves, J. Mech. Phys. Solids **46**, 467 (1998).

[11] J. W. Morrissey and J. R. Rice, Perturbative simulations of crack front waves, J. Mech. Phys. Solids **48**, 1229 (2000).

[12] E. Sharon, G. Cohen, and J. Fineberg, Propagating solitary waves along a rapidly moving crack front, Nature (London) **410**, 68 (2001).

[13] E. Sharon, G. Cohen, and J. Fineberg, Crack front waves and the dynamics of a rapidly moving crack, Phys. Rev. Lett. **88**, 085503 (2002).

[14] J. Fineberg, E. Sharon, and G. Cohen, Crack front waves in dynamic fracture, Int. J. Fract. **121**, 55 (2003).

[15] A. Livne, G. Cohen, and J. Fineberg, Universality and hysteretic dynamics in rapid fracture, Phys. Rev. Lett. **94**, 224301 (2005).

[16] K. Ravi-Chandar, Dynamic fracture of nominally brittle materials, Int. J. Fract. **90**, 83 (1998).

[17] J. Fineberg and M. Marder, Instability in dynamic fracture, Phys. Rep. **313**, 1 (1999).

[18] D. Bonamy and K. Ravi-Chandar, Interaction of shear waves and propagating cracks, Phys. Rev. Lett. **91**, 235502 (2003).

[19] D. Bonamy and K. Ravi-Chandar, Dynamic crack response to a localized shear pulse perturbation in brittle amorphous materials: On crack surface roughening, Int. J. Fract. **134**, 1 (2005).

[20] T. Baumberger, C. Caroli, D. Martina, and O. Ronsin, Magic angles and cross-hatching instability in hydrogel fracture, Phys. Rev. Lett. **100**, 178303 (2008).

[21] H. Henry, Study of three-dimensional crack fronts under plane stress using a phase field model, Europhys. Lett. **92**, 46002 (2010).

[22] A. Pons and A. Karma, Helical crack-front instability in mixed-mode fracture, Nature (London) **464**, 85 (2010).

[23] H. Henry and M. Adda-Bedia, Fractographic aspects of crack branching instability using a phase-field model, Phys. Rev. E **88**, 060401(R) (2013).

[24] J. Willis, Crack front perturbations revisited, Int. J. Fract. **184**, 17 (2013).

[25] M. Adda-Bedia, R. E. Arias, E. Bouchbinder, and E. Katzav, Dynamic stability of crack fronts: Out-of-plane corrugations, Phys. Rev. Lett. **110**, 014302 (2013).

[26] C.-H. Chen, T. Cambonie, V. Lazarus, M. Nicoli, A. J. Pons, and A. Karma, Crack front segmentation and facet coarsening in mixed-mode fracture, Phys. Rev. Lett. **115**, 265503 (2015).

[27] I. Kolvin, G. Cohen, and J. Fineberg, Crack front dynamics: The interplay of singular geometry and crack instabilities, Phys. Rev. Lett. **114**, 175501 (2015).

[28] J. Bleyer, C. Roux-Langlois, and J.-F. Molinari, Dynamic crack propagation with a variational phase-field model: limiting speed, crack branching and velocity-toughening mechanisms, Int. J. Fract. **204**, 79 (2017).

[29] J. Bleyer and J.-F. Molinari, Microbranching instability in phase-field modelling of dynamic brittle fracture, Appl. Phys. Lett. **110**, 151903 (2017).

[30] I. Kolvin, J. Fineberg, and M. Adda-Bedia, Nonlinear focusing in dynamic crack fronts and the microbranching transition, Phys. Rev. Lett. **119**, 215505 (2017).

[31] I. Kolvin, G. Cohen, and J. Fineberg, Topological defects govern crack front motion and facet formation on broken surfaces, Nat. Mater. **17**, 140 (2018).

[32] F. Fekak, F. Barras, A. Dubois, D. Spielmann, D. Bonamy, P. Geubelle, and J. Molinari, Crack front waves: A 3D dynamic response to a local perturbation of tensile and shear cracks, J. Mech. Phys. Solids **135**, 103806 (2020).

[33] T. Roch, M. Lebihain, and J.-F. Molinari, Dynamic crack front deformations in cohesive materials, Phys. Rev. Lett. **131**, 096101 (2023).

[34] W. Steinhardt and S. M. Rubinstein, How material heterogeneity creates rough fractures, Phys. Rev. Lett. **129**, 128001 (2022).

[35] M. Wang, M. Adda-Bedia, J. M. Kolinski, and J. Fineberg, How hidden 3D structure within crack fronts reveals energy balance, J. Mech. Phys. Solids **161**, 104795 (2022).

[36] M. Wang, M. Adda-Bedia, and J. Fineberg, Dynamics of three-dimensional stepped cracks, bistability, and their transition to simple cracks, Phys. Rev. Res. **5**, L012001 (2023).

[37] A. Karma, D. A. Kessler, and H. Levine, Phase-field model of mode III dynamic fracture, Phys. Rev. Lett. **87**, 045501 (2001).

[38] A. Karma and A. E. Lobkovsky, Unsteady crack motion and branching in a phase-field model of brittle fracture, Phys. Rev. Lett. **92**, 245510 (2004).

[39] H. Henry and H. Levine, Dynamic instabilities of fracture under biaxial strain using a phase field model, Phys. Rev. Lett. **93**, 105504 (2004).

[40] V. Hakim and A. Karma, Crack path prediction in anisotropic brittle materials, Phys. Rev. Lett. **95**, 235501 (2005).

[41] H. Henry, Study of the branching instability using a phase field model of inplane crack propagation, Europhys. Lett. **83**, 16004 (2008).

[42] V. Hakim and A. Karma, Laws of crack motion and phase-field models of fracture, J. Mech. Phys. Solids **57**, 342 (2009).

[43] I. S. Aranson, V. A. Kalatsky, and V. M. Vinokur, Continuum field description of crack propagation, Phys. Rev. Lett. **85**, 118 (2000).

[44] L. O. Eastgate, J. P. Sethna, M. Rauscher, T. Cretegny, C. S. Chen, and C. R. Myers, Fracture in mode I using a conserved phase-field model, Phys. Rev. E **65**, 036117 (2002).

[45] See Supplemental Material at http://link.aps.org/supplemental/10.1103/PhysRevE.108.L043002 for additional information, which includes Refs. [4–6,12–14,60].

[46] A. Yuse and M. Sano, Transition between crack patterns in quenched glass plates, Nature (London) **362**, 329 (1993).

[47] M. Marder, Instability of a crack in a heated strip, Phys. Rev. E **49**, R51(R) (1994).

[48] M. Adda-Bedia and Y. Pomeau, Crack instabilities in a heated glass strip, Phys. Rev. E **52**, 4105 (1995).

[49] H. A. Bahr, A. Gerbatsch, U. Bahr, and H. J. Weiss, Oscillatory instability in thermal cracking: A first-order phase-transition phenomenon, Phys. Rev. E **52**, 240 (1995).

[50] E. G. D. Cohen and I. M. deSchepper, Experimental study of quasistatic brittle crack propagation, Phys. Rev. Lett. **75**, 2252 (1995).

[51] B. Yang and K. Ravi-Chandar, Crack path instabilities in a quenched glass plate, J. Mech. Phys. Solids **49**, 91 (2001).

[52] E. Bouchbinder, H. G. E. Hentschel, and I. Procaccia, Dynamical instabilities of quasistatic crack propagation under thermal stress, Phys. Rev. E **68**, 036601 (2003).

[53] F. Corson, M. Adda-Bedia, H. Henry, and E. Katzav, Thermal fracture as a framework for quasistatic crack propagation, Int. J. Fract. **158**, 1 (2009).

[54] A. Livne, O. Ben-David, and J. Fineberg, Oscillations in rapid fracture, Phys. Rev. Lett. **98**, 124301 (2007).

[55] E. Bouchbinder, Dynamic crack tip equation of motion: High-speed oscillatory instability, Phys. Rev. Lett. **103**, 164301 (2009).

[56] T. Goldman, R. Harpaz, E. Bouchbinder, and J. Fineberg, Intrinsic nonlinear scale governs oscillations in rapid fracture, Phys. Rev. Lett. **108**, 104303 (2012).

[57] E. Sharon and J. Fineberg, Confirming the continuum theory of dynamic brittle fracture for fast cracks, Nature (London) **397**, 333 (1999).

[58] A. Livne, E. Bouchbinder, I. Svetlizky, and J. Fineberg, The near-tip fields of fast cracks, Science **327**, 1359 (2010).

[59] F. Célarié, S. Prades, D. Bonamy, L. Ferrero, E. Bouchaud, C. Guillot, and C. Marliere, Glass breaks like metal, but at the nanometer scale, Phys. Rev. Lett. **90**, 075504 (2003).

[60] L. Verlet, Computer "experiments" on classical fluids. I. Thermodynamical properties of Lennard-Jones molecules, Phys. Rev. **159**, 98 (1967).